

Original Full Length Article

Nanometer-scale features on micrometer-scale surface texturing: A bone histological, gene expression, and nanomechanical study



Paulo G. Coelho^a, Tadahiro Takayama^b, Daniel Yoo^a, Ryo Jimbo^{c,*}, Sanjay Karunakaran^d, Nick Tovar^a, Malvin N. Janal^e, Seiichi Yamano^b

^a Department of Biomaterials and Biomimetics, New York University College of Dentistry, New York, NY, USA

^b Department of Prosthodontics, New York University College of Dentistry, New York, NY, USA

^c Department of Prosthodontics, Faculty of Odontology, Malmö University, Malmö, Sweden

^d Department of Prosthodontics, University of Tennessee Health Science Center, College of Dentistry, Memphis, TN, USA

^e Department of Epidemiology and Health Promotion, New York University, New York, NY, USA

ARTICLE INFO

Article history:

Received 1 October 2013

Revised 18 April 2014

Accepted 5 May 2014

Available online 9 May 2014

Edited by: Regis O'Keefe

Keywords:

Nanotopography

Gene expression

Osseointegration

Nanomechanics

ABSTRACT

Micro- and nanoscale surface modifications have been the focus of multiple studies in the pursuit of accelerating bone apposition or osseointegration at the implant surface. Here, we evaluated histological and nanomechanical properties, and gene expression, for a microblasted surface presenting nanometer-scale texture within a micrometer-scale texture (MB) (Ossean™ Surface, Intra-Lock International, Boca Raton, FL) versus a dual-acid etched surface presenting texture at the micrometer-scale only (AA), in a rodent femur model for 1, 2, 4, and 8 weeks in vivo. Following animal sacrifice, samples were evaluated in terms of histomorphometry, biomechanical properties through nanoindentation, and gene expression by real-time quantitative reverse transcription polymerase chain reaction analysis. Although the histomorphometric, and gene expression analysis results were not significantly different between MB and AA at 4 and 8 weeks, significant differences were seen at 1 and 2 weeks. The expression of the genes encoding collagen type I (COL-1), and osteopontin (OPN) was significantly higher for MB than for AA at 1 week, indicating up-regulated osteoprogenitor and osteoblast differentiation. At 2 weeks, significantly up-regulated expression of the genes for COL-1, runt-related transcription factor 2 (RUNX-2), osterix, and osteocalcin (OCN) indicated progressive mineralization in newly formed bone. The nanomechanical properties tested by the nanoindentation presented significantly higher-rank hardness and elastic modulus for the MB compared to AA at all time points tested. In conclusion, the nanotopographical featured surfaces presented an overall higher host-to-implant response compared to the microtextured only surfaces. The statistical differences observed in some of the osteogenic gene expression between the two groups may shed some insight into the role of surface texture and its extent in the observed bone healing mechanisms.

© 2014 Elsevier Inc. All rights reserved.

Introduction

It has been known that [1] moderately micro-roughened surface with an average height deviation (S_a) ranging between 1.0 and 2.0 μm and a developed surface ratio (S_{dr}) of around 50% has been suggested to elicit the most favorable bone responses to the oral implant [2–4]. A method to further increase the bioactivity of the implant is to topographically and chemically modify the surface, and the use of calcium phosphate has shown enhanced bone apposition in numerous in vivo studies [5–8]. However, there have been indications that the application of a thick plasma-sprayed hydroxyapatite coating would potentially provoke clinical complications, such as detachment of the coating and eventual inflammation caused by the released apatite particles [9–11].

In order to improve the mechanical properties of the coated hydroxyapatite to prevent negative biological effects, different coating methodologies have been proposed, which appear to significantly improve the coating bonding properties [6,12–14]. Modifications using resorbable bioceramic grit blasting media have been one of the most promising methodologies showing osteoconductive properties [15,16]. Interestingly, some of those surface treatments have been reported to present both micro- and nanotopographies [13,17–23].

The addition of nanotopography on implant surfaces has shown to result in significantly enhanced osseointegration and has been suggested to affect cellular shape and fate, e.g. apoptosis, growth, and differentiation [24]. Gittens et al. [25] reported enhanced differentiation of pre-osteoblasts with nanoscale modifications through significantly higher levels of osteocalcin (OCN) and osteoprotegerin expression in vitro. Moreover, surface modification using fluoride has been reported to provide nanoscale roughness, which resulted in up-regulated bone-specific gene expression in human mesenchymal stem cells [26].

* Corresponding author at: Department of Prosthodontics, Faculty of Odontology, Malmö University, 205 06 Malmö, Sweden. Fax: +46 40 665 8503.

E-mail address: ryo.jimbo@mah.se (R. Jimbo).

In agreement with the *in vitro* studies, several animal studies utilizing histological or biomechanical evaluation techniques suggested that the presence of nanostructures on implant surfaces accelerated and improved bone formation [1,27,28].

In order to further investigate the effect of nanotopography, Jimbo et al. [29] have investigated gene expression in the newly formed bone proximal to the nanostructured implant, and reported up-regulated osteogenic gene expression with concurrently increased osteoclast activity, indicating the active role played by the nanostructures in bone formation. Furthermore, Hayashi et al. [30], reported that even when histomorphometric evaluation concerning nanomodified implants did not reveal differences between different groups, the gene expression technique revealed that the remodeling activity was significantly higher for a certain nanolevel modification.

Therefore, in this study, we used real-time quantitative reverse transcription polymerase chain reaction (qRT-PCR) to characterize the gene expression of the tissue around microblasted surface presenting nanometer-scale texture within a micrometer-scale texture, and evaluated the differences to a dual-acid etched surface that exhibited texture at the micrometer scale, in tandem with histomorphometric and nano-mechanical analysis using the nanoindenter. It was hypothesized that MB surfaces would present up-regulated osteogenic gene expression compared to the controls, and that the combination of different evaluation techniques would facilitate better interpretation of the biological phenomenon.

Materials and methods

Implant

Two types of titanium implants (4 mm in length by 1.5 mm in diameter, Fig. 1), i.e. a microblasted surface presenting nanometer-scale texture within a micrometer-scale texture (MB), Ossean™ Surface, and a dual-acid etched surface presenting texture at the micrometer-scale only (AA), were provided by an implant manufacturer (Intra-Lock International, Boca Raton, FL). Scanning electron micrographs of both surfaces are presented in Fig. 2.

Sample preparation, implantation, and histological evaluation

Animal experiments were conducted with ethical approval from the New York University School of Medicine (protocol #090504-03). A Sprague–Dawley male rat femur model ($n = 40$; 8–10 weeks old, 300–350 grams each) was utilized in the present study. A total of 40 implants of each type were distributed among the experimental and control groups according to the length of time *in vivo* (1, 2, 4, and 8 weeks; $n = 10$ per group). General anesthesia was administered via intramuscular injection with 0.3–0.4 ml of ketamine/xylazine (80–100 mg/kg

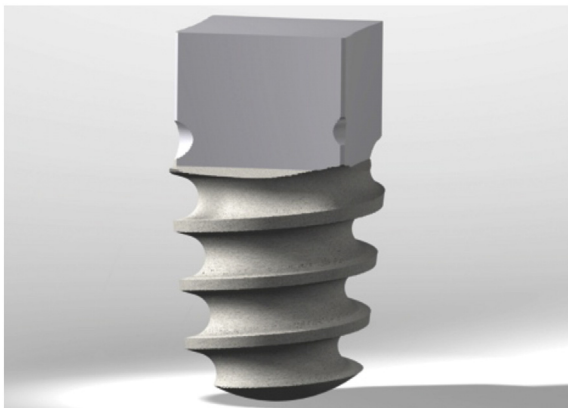


Fig. 1. Implant design utilized in the present study.

and 10–20 mg/kg body weight, respectively). The flat medial surface of the femur was used as the surgical site. The surgical areas were shaved, and the skin was washed with 70% ethanol before surgical draping. The surgical site was exposed with an incision on the medial surface of the femur through the skin, fascia, and periosteum using a sterile surgical blade. The implant osteotomy was prepared using a No. 6 round burr, and all drilling procedures were carried out under profuse sterile saline irrigation. The AA and MB implants were inserted with a self-tapping procedure, in which all of the implants penetrated only the first layer of the bone cortex. A total of two osteotomies on the right side and one on the left side of these rats were performed by placing a screw-shaped MB and a control implant (mock surgery, involving drilling only and no implant) on the right side and an AA implant on the left side. After surgery, the tissues were closed in layers and sutured using 5-0 absorbable sutures (Henry Schein, Melville, NY). Buprenorphine (0.01–0.05 mg/kg) was administered as post-surgery analgesia, injected intramuscularly for 3 days to control postsurgical pain. The implants remained for 1, 2, 4, or 8 weeks *in vivo* ($n = 10$ per group). Upon animal sacrifice, the implants and surrounding bone were retrieved and examined for gene expression levels, histology, and bone mechanical properties. For qRT-PCR, the femurs containing the implants were then placed into Trizol reagent (Invitrogen, Carlsbad, CA) at -80°C . For histology and nanoindentation, the bone samples were stored in 70% ethanol for 24 hours and subsequently washed under running water for an additional 24 hours. The samples then underwent progressive dehydration through a series of alcohol solutions ranging from 70% to 100% ethanol and embedded in a methacrylate-based resin according to the manufacturer's instructions (Technovit 9100, Heraeus Kulzer GmbH, Wehrheim, Germany). The resin blocks were sectioned along the implant long axis with a precision diamond saw (Isomet 2000, Buehler, Lake Bluff, IL) as slices of $\sim 300\ \mu\text{m}$ thickness and glued to an acrylic plate with acrylate-based cement. After allowing the samples 24 hours to set, they were prepared for nanoindentation testing by grinding (400–2400 grit SiC abrasive papers) and polishing (diamond suspension solutions of 1–9 μm particle size; Isomet 2000, Buehler, Lake Bluff, IL) using a grinding/polishing machine (Metaserv 3000, Buehler) under water irrigation to a final thickness of $\sim 50\ \mu\text{m}$. Two sets of implant sections were created for nanoindentation mechanical testing and standardized non-decalcified histology [31]. Histological observations and images were obtained using a light microscope (Leica DM2500M, Leica Microsystems GmbH, Wetzlar, Germany) and specialized computer software (Leica Application Suite, Leica Microsystems GmbH). Using the software, the bone-to-implant contact (BIC) along the implant and the bone area fraction occupancy (BAFO) within the implant thread chambers were calculated.

Nanoindentation testing

Nanoindentation ($n = 30$ per specimen) was performed using a triboindenter (TI 950, Hysitron, Minneapolis, MN) equipped with a Berkovich diamond three-sided pyramid probe. Water droplets were added to the surface of each sample slide upon proper tip and probe calibration for testing under wet conditions. A loading profile was developed with a peak load of 300 μN at a rate of 60 $\mu\text{N/s}$, followed by holding and unloading times of 10 and 2 sec, respectively. The extended holding period allowed sufficient relaxation of the surrounding bone around the testing probe and a more linear relaxing response, which prevented any tissue creep effect during the unloading portion of the loading profile.

For each specimen, mechanical testing was performed within the threaded regions (cortical area) between the first and second plateau or the initial set of inter-plateau spaces containing novel bone formation. If no cortical bone was present within any of the inter-plateau regions, the specimen was discarded. Bone tissue within these regions was initially detected via imaging through a light microscope (Hysitron) [32]. Indentations ($n = 30/\text{implant}$) were performed in the identified regions of interest within each plateau region.

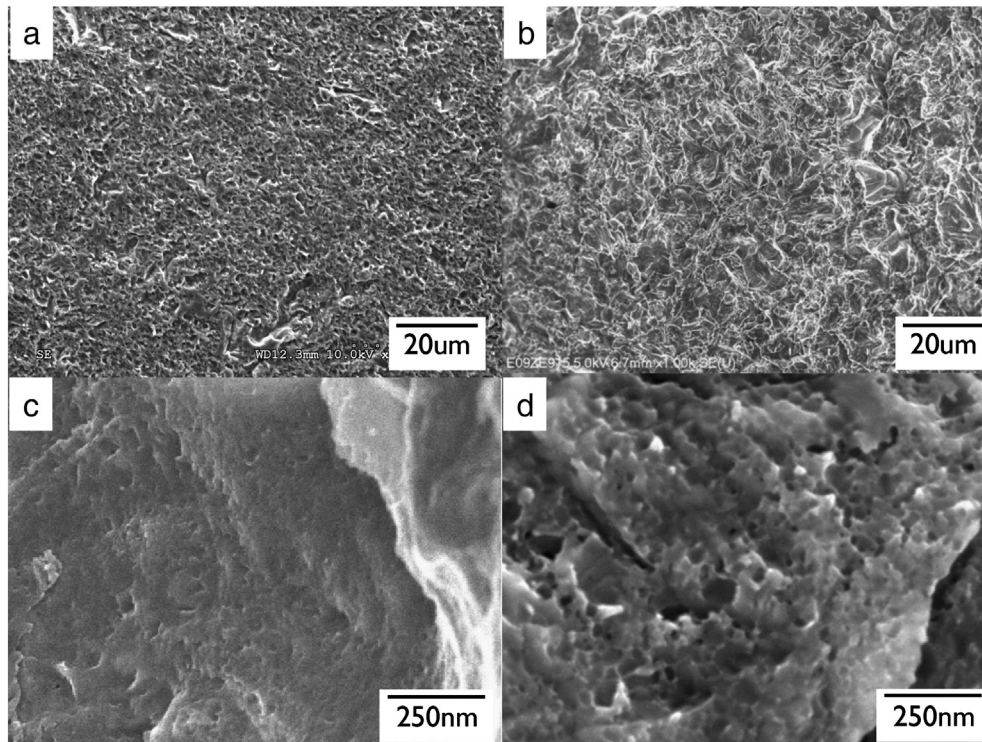


Fig. 2. Scanning electron micrographs of the AA (a and c) and MB (b and d) surfaces.

From each generated load–displacement curve (Fig. 1), the reduced modulus E_r (GPa) and hardness H (GPa) of cortical bone tissue were computed via the Hysitron TriboScan software using the following formulae, respectively:

$$E_r = \frac{\sqrt{\pi}}{2\sqrt{A(h_c)}} \times S; \quad H = \frac{P_{\max}}{A(h_c)}$$

where S is the stiffness, h_c is the contact depth, P_{\max} is the maximum applied force (300 μ N), and $A(h_c)$ is the contact area computed from the TriboScan software utilizing the area function with respect to the contact depth. Through the reduced modulus E_r , the corresponding elastic modulus E_b (GPa) may be calculated using the following equation:

$$\frac{1}{E_r} = \frac{1 - \nu_b^2}{E_b} + \frac{1 - \nu_i^2}{E_i}$$

where ν_b (0.3) is the Poisson's ratio for cortical bone, E_i (1140 GPa) is the elastic modulus of the indenter, and ν_i (0.07) is the Poisson's ratio for the indenter [33,34]. This methodology [35] has been shown successful in determining the mechanical properties of bone through nanoindentation [1,36–39].

RNA extraction and qRT-PCR

RNA from the retrieved samples was extracted from the pulverized bone powder using Trizol reagent according to the manufacturer's protocol. RNA levels were then measured using a NanoDrop ND-1000 Spectrophotometer (NanoDrop Technologies, Wilmington, DE, USA) and treated with DNase I. Rat Universal ProbeLibrary probes and target-specific PCR primers for type I collagen (COL-1), runt-related transcription factor 2 (RUNX-2), osterix, osteopontin (OPN), osteocalcin (OCN), alkaline phosphatase (ALP), and β -actin, a housekeeping gene, were selected using the ProbeFinder assay design software (Table 1). cDNAs were synthesized from 1 μ g of total extracted RNA for each sample using reverse transcriptase (Roche, Nutley, NJ). Reactions were

performed using the 480 LightCycler (Roche) in 20- μ l reaction volumes for the genes encoding COL-1, RUNX-2, osterix, OPN, OCN, ALP and β -actin using 100 ng of cDNA under the following conditions: 95 $^{\circ}$ C for 5 min, 50 cycles at 95 $^{\circ}$ C for 10 sec, 60 $^{\circ}$ C for 15 sec, and 72 $^{\circ}$ C for 1 sec as previously reported [40,41]. To confirm real-time PCR specificity, gel electrophoretic assessment was performed (data not shown). Each product size of PCR was the following (unit bp): COL-1, 106; RUNX-2, 150; Osterix, 166; OPN, 216; OCN, 354; ALP, 183; and β -actin: 150. The comparative Ct method (also as known the $2^{-\Delta\Delta Ct}$ method) was used to obtain quantitative data of relative gene expression. The qRT-PCR results of the experimental genes were normalized against an internal control group, β -actin. Triplicates for each data set were averaged, and the mean values were used for statistical analysis.

Statistical analysis

The collected dependent variables and histomorphometric data, i.e. BIC, BAFO, rank hardness (GPa), and rank elastic modulus (GPa), were displayed as estimated means with their respective 95% confidence intervals (95% CI) and utilized to generate a general linear analysis of variance (ANOVA) model (NCSS LLC) with the level of significance

Table 1
Primer sequences for QRT-PCR.

COL-1	Forward	CCTGAGCCAGCAGATTGA
RUNX-2	Reverse	TCCGCTCTCCAGTCAG
	Reverse	CTGGCTTGGATTAGGGAGTCAC
Osterix	Forward	CGGCAAGGCTTCGCATCTG
	Reverse	GGAGCAGAGCAGACAGGTGAACT
OPN	Forward	GACAGCAACGGGAAGACC
	Reverse	CAGGCTGGCTTTGGAATC
OCN	Forward	GAGGCGAGTAAGGTGGTGAA
	Reverse	CGTCCTGGAAGCCAATGTG
ALP	Forward	AGCGACACGGACAAGAAGC
	Reverse	GGCAAAGACCGCCACATC
β -Actin	Forward	GGAGATTACTGCCCTGGCTCTCA
	Reverse	GACTCATCGTACTCTGCTTGCTG

set at $p < 0.05$. The rank hardness and elastic modulus were utilized for the analysis since preliminary nanoindentation data analysis showed deviations from normality that was corrected by ranking the outcome from the lowest to highest values [1,36–39]. The independent variables included the implant surface type and time in vivo. For gene expression analysis, an ANOVA test was performed to evaluate differences within the data between the groups. p -values less than 0.05 were considered significant.

Results

Histological observations

The histological sections revealed newly formed trabeculae with deeply stained mineralized tissue for both groups after 1 and 2 weeks of healing, with no visible differences in bone formation between the groups (Fig. 3). At 4 and 8 weeks, the woven bone observed at the 1- and 2-week time-points was replaced by lamellar bone in close proximity with the implant surface.

Histomorphometric analysis

Significant differences ($p < 0.02$) in bone-to-implant contact (BIC) were seen between the MB and AA implants at 1 and 2 weeks in vivo, with the MB implant group showing higher results (Fig. 4). No BIC significant difference was observed at 4 weeks ($p > 0.35$), as well as at 8 week ($p > 0.25$). No differences in bone area fraction occupancy (BAFO) levels were detected between the groups at 1 and 4 weeks ($p > 0.80$ and $p > 0.91$, respectively). At 2 weeks in vivo, the AA group presented significantly higher values than the MB group ($p < 0.03$) (Fig. 4). At 8 weeks in vivo, the MB group presented a significantly higher BAFO value compared to the AA group ($p < 0.04$) (Fig. 4).

Biomechanical characterization and nanoindentation evaluation

Significant differences in either rank hardness (Fig. 5) or rank elastic modulus (Fig. 6) were observed between the MB and AA implant groups when time in vivo ($p = 0.03$, $p < 0.02$, respectively; Figs. 5 and 6) was considered. When implant surface type was considered, the MB group presented significantly higher-rank hardness and ranks elastic modulus compared to the AA group (both at $p < 0.01$) (Figs. 5 and 6). When implant surface group and time in vivo were evaluated together,

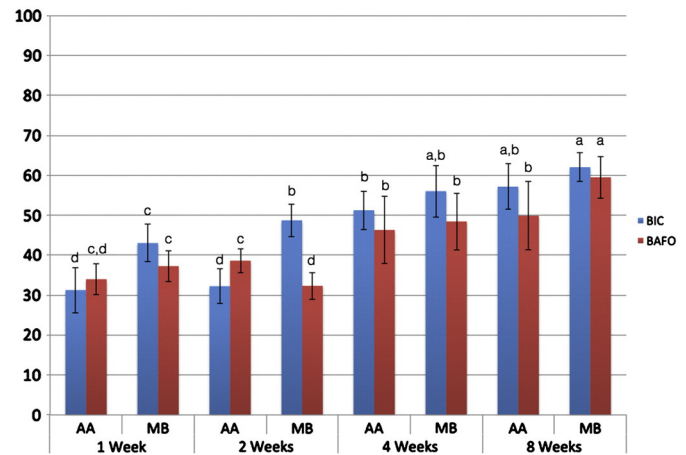


Fig. 4. Statistical summary (mean \pm 95% CI) for %BIC and %BAFO for the MB and AA surfaces at 1, 2, 4, and 8 weeks in vivo. The letters depict statistically homogeneous groups.

significantly higher values of rank hardness and rank elastic modulus were observed for MB implants over those of the AA samples at all times in vivo ($p < 0.02$ and $p < 0.02$, respectively) (Figs. 5 and 6).

Gene expression analysis

The qRT-PCR results are presented in Fig. 7. At 1 week, the expression levels of collagen type 1 (COL-1; 3.8-fold), runt-related transcription factor 2 (RUNX-2; 6.3-fold), OPN (5.1-fold), OCN (1.9-fold), and ALP (4.4-fold) on MB surfaces were significantly higher than those on the unmodified control surface. Within the same time-point, the AA surface induced significantly higher expression of RUNX-2 (3.8-fold) and ALP (3.2-fold) than seen on the control surface. However, within the experimental groups, MB implants exhibited enhanced expression levels of COL-1 (2.1-fold) and OPN (2.5-fold) over those seen in AA implants. At 2 weeks, the expression levels of COL-1 (6.0-fold), RUNX-2 (3.0-fold), osterix (9.0-fold), and OCN (7.4-fold) on MB surfaces were significantly higher than in the control group. Within the same time-point, the AA implants induced significantly higher expression of COL-1 (3.4-fold), OPN (1.8-fold), and ALP (2.0-fold) than on control surfaces. However, within the experimental groups, MB surfaces enhanced

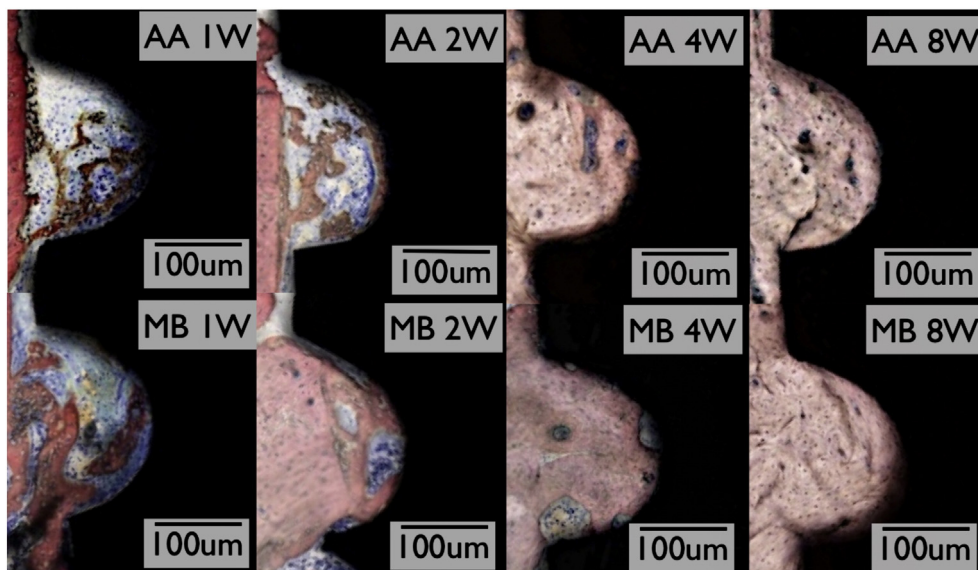


Fig. 3. Histological sections for the MB and AA groups at 1, 2, 4, and 8 weeks in vivo.

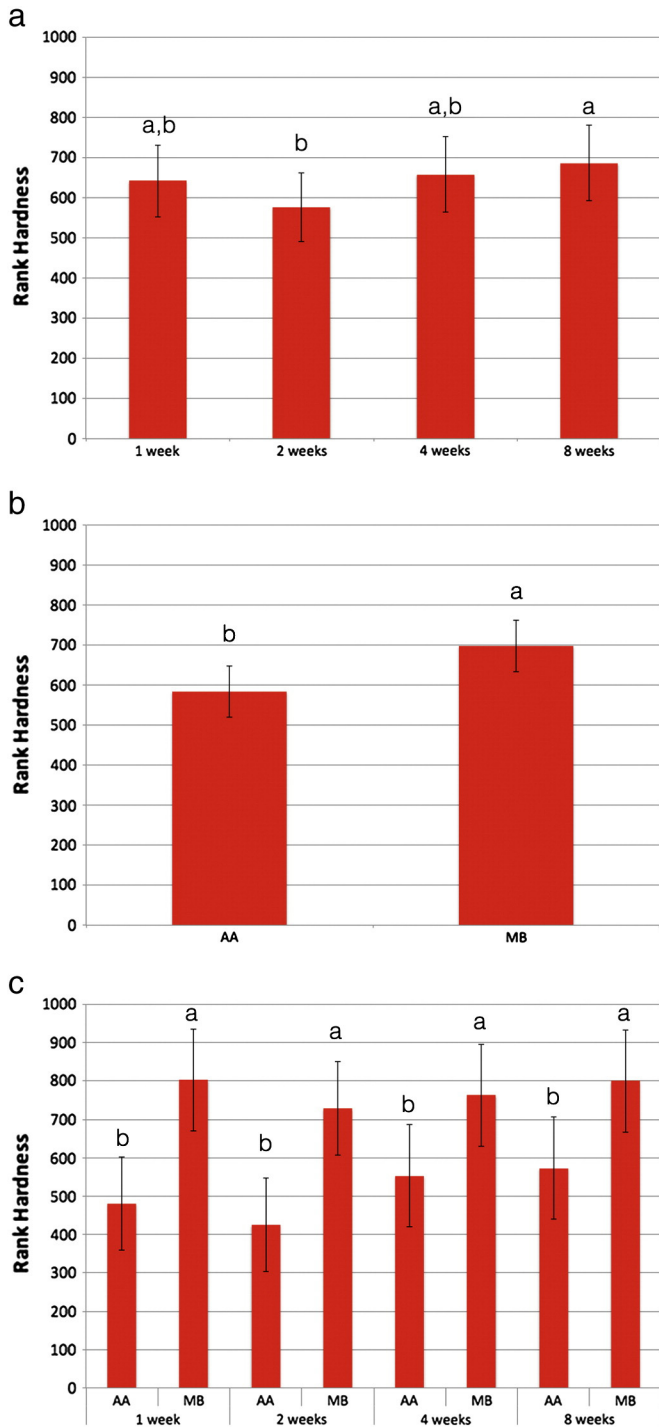


Fig. 5. Statistical results summary (mean \pm 95% CI) of rank hardness values with respect to implant surface and time in vivo: (a) time in vivo; (b) implant surface; (c) time in vivo and implant surface. The letters depict statistically homogeneous groups.

COL-1 (1.8-fold), RUNX-2 (2.3-fold), osterix (6.3-fold), and OCN (2.5-fold) expression in comparison to the AA samples. No differences in gene expression level were detected between the groups at 4–8 weeks (data not shown).

Discussion

Traditional methods of determining the extent of osseointegration in a quantitative manner primarily depend on histology/histomorphometry and biomechanics. However, in order to compensate for the inherent

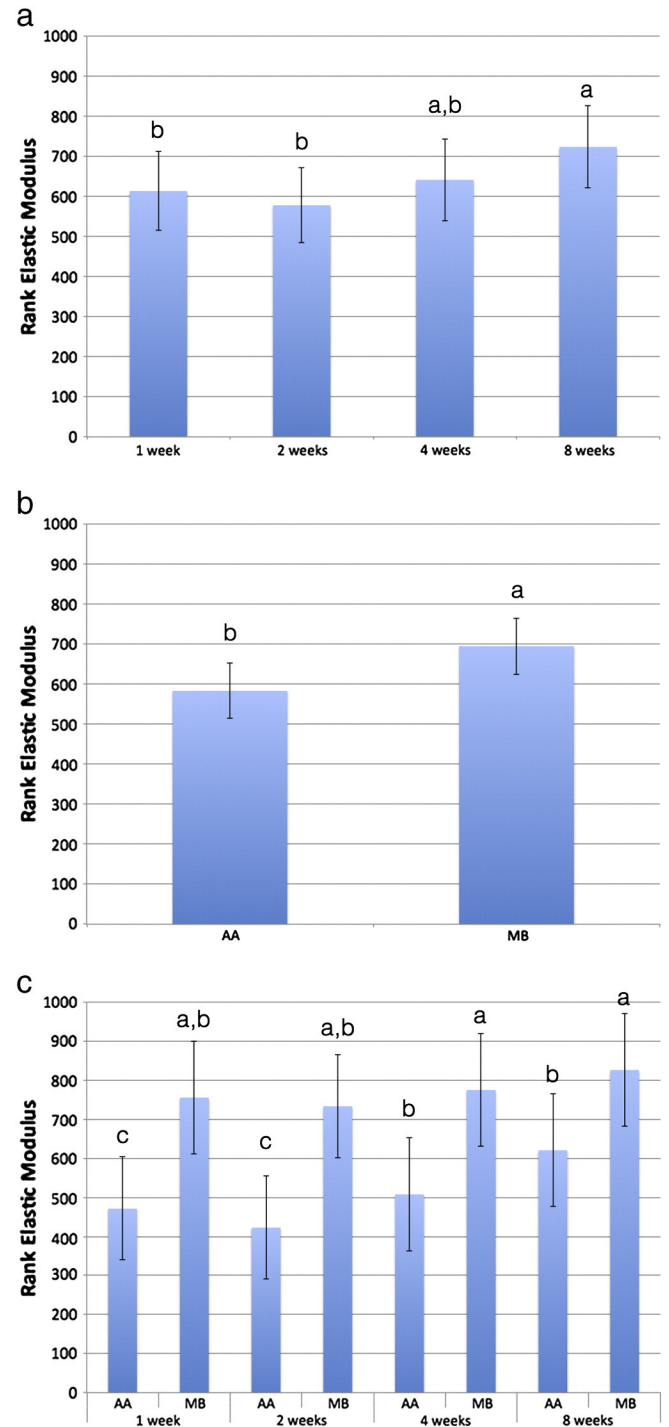


Fig. 6. Statistical results summary (mean \pm 95% CI) of rank elastic modulus values with respect to implant surface and time in vivo: (a) time in vivo; (b) implant surface; (c) time in vivo and implant surface. The letters depict statistically homogeneous groups.

insensitivity in nanoscale detection of the listed techniques, more detailed approaches are essential to elucidate and clarify the roles of the introduced nanopopography. Thus, in addition to nanomechanical characterization of the novel bone tissue in the proximity of the implant, this study investigated the gene expression to a nanostructured bioceramic grit blasted surface and a dual acid-etched surface in a rodent model. One of the major aims of the present study was to unveil the underlying molecular processes corresponding to the observed biomechanics. Based on similar conducted studies, nanopopographical features may initialize acceleration of bone healing at earlier times and have less impact

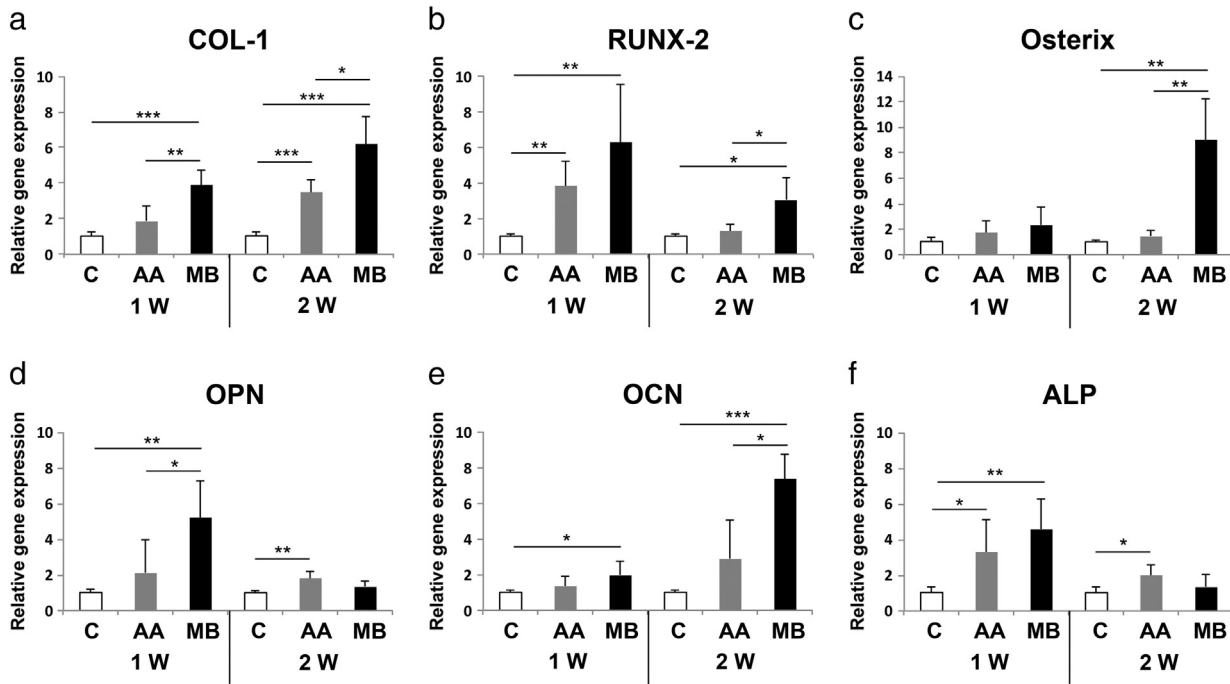


Fig. 7. Gene expression levels of selected markers quantified via real-time RT-PCR. The osteogenic markers, COL-1 (a), RUNX-2 (b), osterix (c), OPN (d), OCN (e), and ALP (f) were analyzed. Note that the number of asterisks depicts specific *p*-values (**p* < 0.05, ***p* < 0.01, and ****p* < 0.001).

on extended healing periods [27,42,43]. We hypothesized that the gene expression would significantly differ between different groups at the early stages of bone formation. When also considering the innate healing time frames of the rodent model, we focused in particular on the evaluation of the gene expression at 1 and 2 weeks, as both BIC and rank hardness/modulus showed higher values for the MB surface as early as 1 and 2 weeks in vivo.

The interaction between cells and microtopographies has been extensively studied. It has been suggested that microtopographies can promote bone-to-implant contact via such mechanisms as mechanical interlocking [44] and enhancement of osteoblast functions by these microtopographies [45]. Nanotopographies have function in promoting cell and tissue growth [46]. Because of the above reasons, some of developed technologies using microtopographies including micro/nano-textured surface topographies have been commercially used to be beneficial for implant osseointegration [47,48]. One of the most important features for enhancement of osseointegration is to balance the relationship between cell proliferation and cell differentiation, simultaneously stimulating both events [49]. Faster cell differentiation may result in faster bone maturation around the implant and offer more promise in bone implant bonding (probably inducing better osseointegration). Furthermore, gene expression is controlled at local levels of implant surface, which may, in part, explain different bone formation profiles on different surface topographies and up-regulated expression of osteogenesis- and extracellular-related genes has been seen during bone healing with titanium implants [50]. A similar gene modulation was found when osteoblasts were cultured on titanium substrates with various microtopographies [51]. In the present study, we demonstrated that MB significantly induced expression of osteogenesis-related genes compared to AA, in the early healing periods 1–2 weeks. This may suggest that MB significantly enhanced cell proliferation and cell differentiation of osteogenesis-related cells compared to AA.

During the osseointegration cascades in bone, a sufficient recruitment of osteogenic cells to the implant surface is the first essential step to initiate a favorable bone healing process in the interfacial zone between bone and implant [52]. Both the resident osteoprogenitor

cells in the peri-implant bone tissue and exogenous mesenchymal cells newly recruited to the implant surface via the local circulation participate in the bone healing of implants in bone [53]. Thus, enhancement in the migration, spreading, and ultimately osteoblast differentiation of osteoprogenitor cells on the implant surface are essential prerequisites for achieving favorable osseointegration. In previous studies, Sr-incorporated Ti oxide surface notably up-regulated mRNA expression of osteoblast genes (Runx2, Osterix, BSP, and OC) in the peri-implant bone tissue at 2 weeks of healing [54]. Also, it was found that the osteogenesis-related gene expressions promoting osteogenesis and relating to osseointegration of COL-1, ALP, and OC were remarkably up-regulated on nanoroughened surfaces at 1 and 2 weeks [55]. Similarly, the present study showed that gene expression levels of osteogenic markers significantly increased in MB at 1 and 2 weeks compared to AA though there was no difference in gene expression between both groups at 4 and 8 weeks. At 1 week, the tissue surrounding the MB peri-implant surface displayed significantly higher expression of COL-1, RUNX-2, OPN, OCN, and ALP relative to the tissue around the control groups. These results indicate that MB surfaces promoted greater osteoprogenitor activity and provided sufficient indication of early bone formation. At 2 weeks, the expression levels of COL-1, RUNX-2, osterix, and OCN were significantly higher for the MB group than for the controls. The up-regulation of COL-1 and osterix indicates osteoblast differentiation and of OCN does indicate mineralization of the surrounding bone tissue [30,56–58]. In particular, osterix expression was notably higher for the MB group at 2 weeks compared to the other groups; this is a strong sign of osteoblast differentiation being significantly influenced by the nanostructures. Moreover, the temporal expression and maturation of extracellular matrix proteins, i.e. fibronectin are essential processes for mineralization [59]. In combination with osteocalcin as a strong indicator of late stage of osteoblast differentiation and mineralization [60,61], these results suggest the acceleration of bone formation and mineralization for the MB group. RUNX-2 is known as a vital transcription factor in osteoblast differentiation [62] and is located upstream to osterix [63], OPN, and OCN [64]. ALP is known to be a regulatory factor for matrix mineralization, and is expressed at the

early stages of osteogenesis [65,66]. The gene expression results of the current study are in accordance with a report by Zhao et al. [48], which demonstrated that surfaces with only microtextures suppressed the expression of markers related to proliferation, intracellular total protein synthesis, alkaline phosphatase (ALP) activity, extracellular matrix deposition and mineralization, whereas hierarchical micro- and nanotextured surfaces caused significant up-regulation of the these factors.

In summary, this study demonstrates significant osteogenic gene up-regulation of the mineralization process that was also detected with BIC histometric measurements and bone mechanical property assessment through nanoindentation. The conventional techniques such as the removal torque testing can be affected not only by the micro-features, but also by the macro-features of the implant (for example, the cutting edge, or the thread shape). Although this is a comprehensive mode of analysis to evaluate the binding between the implant and the supporting tissue, several studies show that the evaluation of the nano-features can be difficult, since other factors have a much larger effect on the reverse torque [29,67]. It can be said that the nanomechanical characterization provides a possibility to purely evaluate the bone mechanical properties in the reduced scale level without the disturbance of other influential factors.

It is evident that the degree of mineralization (hardness and modulus) of the bone in the proximity of the implant was significantly enhanced for the MB surface group at the early in vivo time points. Interestingly, while significant differences in gene expression levels were observed at the two earlier time-points, no differences in gene expression were observed between MB and AA surfaces at 4 and 8 weeks in vivo, suggesting that the overall higher (not necessarily significant at all instances) BIC and BAFO values observed for the MB relative to the AA surface at 4 and 8 weeks in vivo possibly resulted from the wound healing pathway alteration tracked by gene expression at earlier implantation times. Altogether, these results suggest that this may be an important influential factor for the mineralization of the surrounding bone. At longer healing periods, remodeling procedures may be more prominent than osteogenesis [68]. Since remodeling is regulated by both local and systemic factors, investigating the gene expression of regulatory factors such as insulin-like growth factor 1, transforming growth factor β , or interleukins may provide further information concerning gene expression characteristics over longer healing periods [68].

Conclusion

Microblasted implant surfaces possessing hierarchical micro- and nanotextures have been reported in biomechanical and histomorphometric studies to positively influence early healing and mechanical fixation within the host model. In order to compensate or avoid the inherent insensitivity of current evaluation techniques, this study combined the nanomechanical characterization, qualitative histology, and gene expression properties of specific osteogenic markers to further characterize the proper relationship between bone response and surface topographical or chemical features. The combination of these techniques revealed some of the more intricate biochemical relationships and corresponding nanomechanical responses for the enhanced osteoblastic activity and de novo bone formation seen on the MB surface at early healing periods. Future studies considering alternative osteoblastic and osteoclastic markers with nanoindentation analysis of additional time-points are warranted.

Acknowledgments

This study was partially supported by Intra-Lock International, Boca Raton, Florida, the American College of Prosthodontists Education Foundation—Research Fellowship in Prosthodontics, The Northeastern Gnathological Society—Granger-Pruden Award, and The Academy of Prosthodontics—Research Grant Award to Sanjay Karunagar.

References

- [1] Jimbo R, Coelho PG, Bryington M, Baldassarri M, Tovar N, Currie F, et al. Nano hydroxyapatite-coated implants improve bone nanomechanical properties. *J Dent Res* 2012;91:1172–7.
- [2] Albrektsson T, Wennerberg A. Oral implant surfaces: part 2—review focusing on clinical knowledge of different surfaces. *Int J Prosthodont* 2004;17:544–64.
- [3] Albrektsson T, Wennerberg A. Oral implant surfaces: part 1—review focusing on topographic and chemical properties of different surfaces and in vivo responses to them. *Int J Prosthodont* 2004;17:536–43.
- [4] Wennerberg A, Albrektsson T. On implant surfaces: a review of current knowledge and opinions. *Int J Oral Maxillofac Implants* 2010;25:63–74.
- [5] Hulshoff JE, van Dijk K, van der Waerden JP, Wolke JG, Kalk W, Jansen JA. Evaluation of plasma-spray and magnetron-sputter Ca-P-coated implants: an in vivo experiment using rabbits. *J Biomed Mater Res* 1996;31:329–37.
- [6] Coelho PG, Freire JN, Granato R, Marin C, Bonfante EA, Gil JN, et al. Bone mineral apposition rates at early implantation times around differently prepared titanium surfaces: a study in beagle dogs. *Int J Oral Maxillofac Implants* 2011;26:63–9.
- [7] Junker R, Manders PJ, Wolke J, Borisov Y, Jansen JA. Bone-supportive behavior of microplasma-sprayed CaP-coated implants: mechanical and histological outcome in the goat. *Clin Oral Implants Res* 2010;21:189–200.
- [8] Giavarese G, Fini M, Cigada A, Chiesa R, Rondelli G, Rimondini L, et al. Histomorphometric and microhardness assessments of sheep cortical bone surrounding titanium implants with different surface treatments. *J Biomed Mater Res A* 2003;67:112–20.
- [9] Albrektsson T. Hydroxyapatite-coated implants: a case against their use. *J Oral Maxillofac Surg* 1998;56:1312–26.
- [10] Johnson BW. HA-coated dental implants: long-term consequences. *J Calif Dent Assoc* 1992;20:33–41.
- [11] Gottlander M, Johansson CB, Albrektsson T. Short- and long-term animal studies with a plasma-sprayed calcium phosphate-coated implant. *Clin Oral Implants Res* 1997;8:345–51.
- [12] Mendes VC, Moineddin R, Davies JE. The effect of discrete calcium phosphate nanocrystals on bone-bonding to titanium surfaces. *Biomaterials* 2007;28:4748–55.
- [13] Yang Y, Kim KH, Ong JL. A review on calcium phosphate coatings produced using a sputtering process—an alternative to plasma spraying. *Biomaterials* 2005;26:327–37.
- [14] Lacefield WR. Current status of ceramic coatings for dental implants. *Implant Dent* 1998;7:315–22.
- [15] Coelho PG, Granato R, Marin C, Jimbo R, Lin S, Witek L, et al. Effect of Si addition on Ca- and P-impregnated implant surfaces with nanometer-scale roughness: an experimental study in dogs. *Clin Oral Implants Res* 2012;23:373–8.
- [16] Bonfante EA, Granato R, Marin C, Jimbo R, Giro G, Suzuki M, et al. Biomechanical testing of microblasted, acid-etched/microblasted, anodized, and discrete crystalline deposition surfaces: an experimental study in beagle dogs. *Int J Oral Maxillofac Implants* 2013;28:136–42.
- [17] Coelho PG, Granato R, Marin C, Bonfante EA, Janal MN, Suzuki M. Biomechanical and bone histomorphologic evaluation of four surfaces on plateau root form implants: an experimental study in dogs. *Oral Surg Oral Med Oral Pathol Oral Radiol Endod* 2010;109:e39–45.
- [18] Burgess AV, Story BJ, Wagner WR, Trisi P, Pikos MA, Guttenberg SA. Highly crystalline MP-1 hydroxylapatite coating. Part II: in vivo performance on endosseous root implants in dogs. *Clin Oral Implants Res* 1999;10:257–66.
- [19] Coelho PG, Suzuki M. Evaluation of an IBAID thin-film process as an alternative method for surface incorporation of bioceramics on dental implants: a study in dogs. *J Appl Oral Sci* 2005;13:87–92.
- [20] Lemons JE. Biomaterials, biomechanics, tissue healing, and immediate-function dental implants. *J Oral Implantol* 2004;30:318–24.
- [21] Ong JL, Carnes DL, Bessho K. Evaluation of titanium plasma-sprayed and plasma-sprayed hydroxyapatite implants in vivo. *Biomaterials* 2004;25:4601–6.
- [22] Orsini G, Piattelli M, Scarano A, Petrone G, Kenealy J, Piattelli A, et al. Randomized, controlled histologic and histomorphometric evaluation of implants with nanometer-scale calcium phosphate added to the dual acid-etched surface in the human posterior maxilla. *J Periodontol* 2007;78:209–18.
- [23] Park YS, Yi KY, Lee IS, Han CH, Jung YC. The effects of ion beam-assisted deposition of hydroxyapatite on the grit-blasted surface of endosseous implants in rabbit tibiae. *Int J Oral Maxillofac Implants* 2005;20:31–8.
- [24] Huang S, Ingber DE. Shape-dependent control of cell growth, differentiation, and apoptosis: switching between attractors in cell regulatory networks. *Exp Cell Res* 2000;261:91–103.
- [25] Gittens RA, McLachlan T, Olivares-Navarrete R, Cai Y, Berner S, Tannenbaum R, et al. The effects of combined micron-/submicron-scale surface roughness and nanoscale features on cell proliferation and differentiation. *Biomaterials* 2011;32:3395–403.
- [26] Guida L, Annunziata M, Rocci A, Contaldo M, Rullo R, Oliva A. Biological response of human bone marrow mesenchymal stem cells to fluoride-modified titanium surfaces. *Clin Oral Implants Res* 2010;21:1234–41.
- [27] Jimbo R, Coelho PG, Vandeweghe S, Schwartz-Filho HO, Hayashi M, Ono D, et al. Histological and three-dimensional evaluation of osseointegration to nanostructured calcium phosphate-coated implants. *Acta Biomater* 2011;7:4229–34.
- [28] Ellingsen JE, Johansson CB, Wennerberg A, Holmen A. Improved retention and bone-to-implant contact with fluoride-modified titanium implants. *Int J Oral Maxillofac Implants* 2004;19:659–66.
- [29] Jimbo R, Xue Y, Hayashi M, Schwartz-Filho HO, Andersson M, Mustafa K, et al. Genetic responses to nanostructured calcium-phosphate-coated implants. *J Dent Res* 2011;90:1422–7.

- [30] Hayashi M, Jimbo R, Xue Y, Mustafa K, Andersson M, Wennerberg A. Photocatalytically induced hydrophilicity influences bone remodelling at longer healing periods: a rabbit study. *Clinical Oral Implants Research* 2014;25:749–54.
- [31] Donath K, Breuner G. A method for the study of undecalcified bones and teeth with attached soft tissues. The Sage–Schliff (sawing and grinding) technique. *J Oral Pathol* 1982;11:318–26.
- [32] Butz F, Aita H, Wang CJ, Ogawa T. Harder and stiffer bone osseointegrated to roughened titanium. *J Dent Res* 2006;85:560–5.
- [33] Hoffer CE, Guo XE, Zysset PK, Goldstein SA. An application of nanoindentation technique to measure bone tissue Lamellae properties. *J Biomech Eng* 2005;127:1046–53.
- [34] Hoffer CE, Moore KE, Kozloff K, Zysset PK, Brown MB, Goldstein SA. Heterogeneity of bone lamellar-level elastic moduli. *Bone* 2000;26:603–9.
- [35] Lee KL, Sobieraj M, Baldassarri M, Gupta N, Pinisetty D, Janal MN, et al. The effects of loading conditions and specimen environment on the nanomechanical response of canine cortical bone. *Mater Sci Eng C Mater Biol Appl* 2013;33:4582–6.
- [36] Jimbo R, Anchieta R, Baldassarri M, Granato R, Marin C, Teixeira HS, et al. Histomorphometry and bone mechanical property evolution around different implant systems at early healing stages: an experimental study in dogs. *Implant Dent* 2013;22:596–603.
- [37] Bougas K, Jimbo R, Vandeweghe S, Tovar N, Baldassarri M, Alenezi A, et al. In vivo evaluation of a novel implant coating agent: laminin-1. *Clin Implant Dent Relat Res* 2013.
- [38] Anchieta RB, Baldassarri M, Guastaldi F, Tovar N, Janal MN, Gottlow J, et al. Mechanical property assessment of bone healing around a titanium–zirconium alloy dental implant. *Clin Implant Dent Relat Res* 2013.
- [39] Baldassarri M, Bonfante E, Suzuki M, Marin C, Granato R, Tovar N, et al. Mechanical properties of human bone surrounding plateau root form implants retrieved after 0.3–24 years of function. *J Biomed Mater Res B Appl Biomater* 2012;100:2015–21.
- [40] Yamano S, Al-Sowighy ZH, Gallucci GO, Wada K, Weber H-P, Sukotjo C. Early peri-implant tissue reactions on different titanium surface topographies. *Clin Oral Implants Res* 2011;22:815–9.
- [41] Yamano S, Haku K, Yamanaka T, Dai J, Takayama T, Shohara R, et al. The effect of a bioactive collagen membrane releasing PDGF or GDF-5 on bone regeneration. *Biomaterials* 2014;35:2446–53.
- [42] Bryington MS, Hayashi M, Kozai Y, Vandeweghe S, Andersson M, Wennerberg A, et al. The influence of nano hydroxyapatite coating on osseointegration after extended healing periods. *Dent Mater* 2013;29:514–20.
- [43] Meirelles L, Arvidsson A, Andersson M, Kjellin P, Albrektsson T, Wennerberg A. Nano hydroxyapatite structures influence early bone formation. *J Biomed Mater Res A* 2008;87:299–307.
- [44] Hansson S, Norton M. The relation between surface roughness and interfacial shear strength for bone-anchored implants. A mathematical model. *J Biomech* 1999;32:829–36.
- [45] Schwartz Z, Nasazky E, Boyan BD. Surface microtopography regulates osteointegration: the role of implant surface microtopography in osteointegration. *Alpha Omega* 2005;98:9–19.
- [46] Liu H, Webster TJ. Nanomedicine for implants: a review of studies and necessary experimental tools. *Biomaterials* 2007;28:354–69.
- [47] Lamolle SF, Monjo M, Rubert M, Haugen HJ, Lyngstadaas SP, Ellingsen JE. The effect of hydrofluoric acid treatment of titanium surface on nanostructural and chemical changes and the growth of MC3T3-E1 cells. *Biomaterials* 2009;30:736–42.
- [48] Zhao L, Mei S, Chu PK, Zhang Y, Wu Z. The influence of hierarchical hybrid micro/nano-textured titanium surface with titania nanotubes on osteoblast functions. *Biomaterials* 2010;31:5072–82.
- [49] Schwartz Z, Olivares-Navarrete R, Wieland M, Cochran DL, Boyan BD. Mechanisms regulating increased production of osteoprotegerin by osteoblasts cultured on microstructured titanium surfaces. *Biomaterials* 2009;30:3390–6.
- [50] Ogawa T, Sukotjo C, Nishimura I. Modulated bone matrix-related gene expression is associated with differences in interfacial strength of different implant surface roughness. *J Prosthodont* 2002;11:241–7.
- [51] Takeuchi K, Saruwatari L, Nakamura HK, Yang JM, Ogawa T. Enhanced intrinsic biomechanical properties of osteoblastic mineralized tissue on roughened titanium surface. *J Biomed Mater Res A* 2005;72:296–305.
- [52] Davies JE. Understanding peri-implant endosseous healing. *J Dent Educ* 2003;67:932–49.
- [53] Xu B, Zhang J, Brewer E, Tu Q, Yu L, Tang J, et al. Osterix enhances BMSC-associated osseointegration of implants. *J Dent Res* 2009;88:1003–7.
- [54] Park J-W, Kim Y-J, Jang J-H, Song H. Positive modulation of osteogenesis- and osteoclastogenesis-related gene expression with strontium-containing microstructured Ti implants in rabbit cancellous bone. *J Biomed Mater Res A* 2013;101A:298–306.
- [55] Kubo K, Tsukimura N, Iwasa F, Ueno T, Saruwatari L, Aita H, et al. Cellular behavior on TiO₂ nanonodular structures in a micro-to-nanoscale hierarchy model. *Biomaterials* 2009;30:5319–29.
- [56] Nakashima K, Zhou X, Kunkel G, Zhang Z, Deng JM, Behringer RR, et al. The novel zinc finger-containing transcription factor osterix is required for osteoblast differentiation and bone formation. *Cell* 2002;108:17–29.
- [57] Miron RJ, Saulacic N, Buser D, Iizuka T, Sculean A. Osteoblast proliferation and differentiation on a barrier membrane in combination with BMP2 and TGFβ1. *Clin Oral Investig* 2012;17:981–8.
- [58] Huang W, Yang S, Shao J, Li YP. Signaling and transcriptional regulation in osteoblast commitment and differentiation. *Front Biosci* 2007;12:3068–92.
- [59] Cowles EA, DeRome ME, Pastizzo G, Brailey LL, Gronowicz GA. Mineralization and the expression of matrix proteins during in vivo bone development. *Calcif Tissue Int* 1998;62:74–82.
- [60] Yonezawa T, Lee JW, Hibino A, Asai M, Hojo H, Cha BY, et al. Harmine promotes osteoblast differentiation through bone morphogenetic protein signaling. *Biochem Biophys Res Commun* 2011;409:260–5.
- [61] Boivin G, Morel G, Lian JB, Antheoine-Terrier C, Dubois PM, Meunier PJ. Localization of endogenous osteocalcin in neonatal rat bone and its absence in articular cartilage: effect of warfarin treatment. *Virchows Arch A Pathol Anat Histopathol* 1990;417:505–12.
- [62] Komori T, Kishimoto T. Cbfa1 in bone development. *Curr Opin Genet Dev* 1998;8:494–9.
- [63] Ma HP, Ming LG, Ge BF, Zhai YK, Song P, Xian CJ, et al. Icaritin is more potent than genistein in promoting osteoblast differentiation and mineralization in vitro. *J Cell Biochem* 2011;112:916–23.
- [64] Pinzone JJ, Hall BM, Thudi NK, Vonau M, Qiang YW, Rosol TJ, et al. The role of Dickkopf-1 in bone development, homeostasis, and disease. *Blood* 2009;113:517–25.
- [65] Suzuki A, Ghayor C, Guicheux J, Magne D, Quillard S, Kakita A, et al. Enhanced expression of the inorganic phosphate transporter Pit-1 is involved in BMP-2-induced matrix mineralization in osteoblast-like cells. *J Bone Miner Res* 2006;21:674–83.
- [66] Hoemann CD, El-Gabalawy H, McKee MD. In vitro osteogenesis assays: influence of the primary cell source on alkaline phosphatase activity and mineralization. *Pathol Biol (Paris)* 2009;57:318–23.
- [67] Breeding K, Jimbo R, Hayashi M, Xue Y, Mustafa K, Andersson M. The effect of hydroxyapatite nanocrystals on osseointegration of titanium implants: an in vivo rabbit study. *Int J Dent* 2014;2014:1–9.
- [68] Watts NB. Clinical utility of biochemical markers of bone remodeling. *Clin Chem* 1999;45:1359–68.